



HAL
open science

Determination of the low energy values of $^{13}\text{CH}_4$ transitions in the $2\nu_3$ region near $1.66 \mu\text{m}$ from absorption spectra at 296 and 81 K

O.M. Lyulin, Samir Kassi, K. Sung, Linda R. Brown, Alain Campargue

► **To cite this version:**

O.M. Lyulin, Samir Kassi, K. Sung, Linda R. Brown, Alain Campargue. Determination of the low energy values of $^{13}\text{CH}_4$ transitions in the $2\nu_3$ region near $1.66 \mu\text{m}$ from absorption spectra at 296 and 81 K. *Journal of Molecular Spectroscopy*, 2010, 261 (2), pp.91-100. 10.1016/j.jms.2010.03.008 . hal-00563124

HAL Id: hal-00563124

<https://hal.science/hal-00563124>

Submitted on 7 Feb 2011

HAL is a multi-disciplinary open access archive for the deposit and dissemination of scientific research documents, whether they are published or not. The documents may come from teaching and research institutions in France or abroad, or from public or private research centers.

L'archive ouverte pluridisciplinaire **HAL**, est destinée au dépôt et à la diffusion de documents scientifiques de niveau recherche, publiés ou non, émanant des établissements d'enseignement et de recherche français ou étrangers, des laboratoires publics ou privés.

Determination of the low energy values of $^{13}\text{CH}_4$ transitions in the $2\nu_3$ region near $1.66\ \mu\text{m}$ from absorption spectra at 296 and 81 K

O. M. Lyulin^{a,c}, S. Kassi^a, K. Sung^b, L.R. Brown^b, and A. Campargue^{a*}

^a *Laboratoire de Spectrométrie Physique (associated with CNRS, UMR 5588), Université Joseph Fourier de Grenoble, B.P. 87, 38402 Saint-Martin-d'Hères Cedex, France.*

^b *Jet Propulsion Laboratory, California Institute of Technology, Mailstop 183-601, 4800 Oak Grove Drive, Pasadena, CA 91109, USA*

^c *Laboratory of Theoretical Spectroscopy, Institute of Atmospheric Optics, Siberian Branch, Russian Academy of Sciences, 1, Akademicheskii av., 634055 Tomsk, Russia*

Number of figures: 9

Number of Tables: 5

Running Head: *Temperature dependence of $^{13}\text{CH}_4$ absorption near $1.66\ \mu\text{m}$*

Keywords: *methane; CH_4 ; $^{13}\text{CH}_4$; absorption spectroscopy; HITRAN; GOSAT, empirical lower states, intensities, positions, quantum assignments*

* Corresponding author: Alain.Campargue@ujf-grenoble.fr

Abstract

The high resolution absorption spectra of $^{13}\text{CH}_4$ were recorded at 81 K by differential absorption spectroscopy using a cryogenic cell and a series of Distributed Feed Back (DFB) diode lasers and at room temperature by Fourier transform spectroscopy. The investigated spectral region corresponds to the high energy part of the $^{13}\text{CH}_4$ tetradecad dominated by the $2\nu_3$ overtone near 5988 cm^{-1} . Empirical line lists were constructed containing, respectively, 1629 $^{13}\text{CH}_4$ transitions detected at 81 K ($5852\text{-}6124\text{ cm}^{-1}$) and 3481 features (including 85 lines of $^{12}\text{CH}_4$) measured at room temperature ($5850\text{-}6150\text{ cm}^{-1}$); the smallest measured intensities are about 3×10^{-26} and 4×10^{-25} cm/molecule at 81 K and 296 K, respectively. The lower state energy values were derived for 1196 $^{13}\text{CH}_4$ transitions from the variation of the line intensities between 81 K and 296 K. These transitions represent 99.2% and 84.6 % of the total absorbance in the region, at 81 K and 296 K respectively. Over four hundred additional weak features were measured at 81 K and could not be matched to lines observed at room temperature. The quality of the resulting empirical low energy values is demonstrated by the excellent agreement with the already-assigned transitions and the clear propensity of the empirical low J values to be close to integers. The two line lists at 81 K and at 296 K provided as Supplementary Material will enable future theoretical analyses of the upper $^{13}\text{CH}_4$ tetradecad.

1. INTRODUCTION

At room temperature, the near infrared spectrum of methane is particularly congested as a result of the complex structure of the rovibrational levels affected by numerous interactions. This is mainly due to the high symmetry of this tetrahedral molecule which leads to many degeneracies and an intricate vibrational structure. In fact, the $3 \times 5 - 6 = 9$ normal vibrational modes correspond to only four fundamental vibration frequencies (three of them being degenerate). In addition, they obey a simple approximate relation $\nu_1 \approx \nu_3 \approx 2\nu_2 \approx 2\nu_4$ between the stretching and bending harmonic frequencies leading to a polyad structure. As a result, the vibrational levels corresponding to the same number, $P = 2V_s + V_b = 2(V_1 + V_3) + (V_2 + V_4)$ have close energy values and constitute a polyad of levels in strong interaction. The number of vibrational levels in a given polyad increases rapidly with the energy, considerably complicating the analysis. Thus, despite important experimental and theoretical efforts, a satisfactory interpretation of near infrared methane still remains elusive. For the main isotopologue, $^{12}\text{CH}_4$, systematic identification is only available up through the octad region at $2.3 \mu\text{m}$ ($P = 3$ – with 8 levels and 24 sublevels) [1] and significant progress has been achieved [2] only very recently in the tetradecad region ($P = 4$ with 14 levels, 60 sublevels) which extends between 4900 and 6200 cm^{-1} . For the $^{13}\text{CH}_4$ species, only the lower polyads up to 3200 cm^{-1} are satisfactorily understood [3] to the extent that observed positions and intensities can be reproduced at or close to experimental uncertainties. As a result, the representation of $^{13}\text{CH}_4$ absorptions at $1.67 \mu\text{m}$ in the public databases [4,5] has been marginal for 25 years. Some 93 positions first introduced in 1986 [6] assumed calculated line intensities of the main isotopologue scaled by the values from Fox *et al.* [7,8]. Later measurements of Margolis [9,10] replaced some of the assigned $^{13}\text{CH}_4$ lines of $2\nu_3$ if intensities were greater than $4 \times 10^{-24} \text{ cm/molecule}$ at room temperature.

The present contribution is devoted to the analysis of the $^{13}\text{CH}_4$ absorption spectrum in the high energy part of the tetradecad dominated by the $2\nu_3$ band centered at 5988 cm^{-1} . Being the strongest band in the region and located at the “edge” of the tetradecad, $2\nu_3$ is less subject to perturbations and has the regular P, Q and R branch structure seen in the ν_3 fundamental near 3018 cm^{-1} . Thirty years ago, Fox *et al.* [7,8] assigned the F2 component of $2\nu_3$ up to $J = 8$ and determined the spectroscopic constants using absorption spectrum recorded with a grating spectrometer and a 4.28 m optical path. The prevalent assumption that isotopic substitution of the central carbon atom would not significantly affect the intensities of the transitions in $^{12}\text{CH}_4$ and $^{13}\text{CH}_4$ was challenged by their $2\nu_3$ intensity measurements [8]. From their

experiment dedicated to the measurements of the relative intensities of the Q₁, R₀ and R₁ in ¹²CH₄ and ¹³CH₄, Fox *et al.* concluded that the ¹²CH₄ line strengths were stronger by more than 30%. This “anomalous” line strength ratio was confirmed by Varanasi [11] from a series of spectra recorded at low temperatures down to 100 K.

The tetradecad, with 14 bands with a total of 60 sub-vibrational states, gives rise to the strong 2ν₃ band and numerous weaker transitions between 4800 and 6200 cm⁻¹. It should be noted that half of the 60 sub-states are not nominally infrared active and must borrow intensity to be observed in absorption. Very recently, Nikitin *et al.* performed a very enlightening comparative study of this polyad for both ¹²CH₄ and ¹³CH₄ [12]. It revealed a one-to-one correspondence between the lines of the strong bands of the two isotopologues, the ¹³CH₄ bands being shifted by a constant value varying between 6 and 30 cm⁻¹ according to the vibrational band. These authors used the isotopic shifts to establish the identification of 339 stronger transitions between 5553 and 6114 cm⁻¹ in both ¹²CH₄ and ¹³CH₄ with new identifications of ν₂+ν₃+ν₄ near 5830 cm⁻¹, 2ν₂+ν₃ near 6060 cm⁻¹ and the E component of 2ν₃ near 6030 cm⁻¹. Furthermore, the isotopic shifts between the ¹²CH₄ and ¹³CH₄ vibrational levels were computed from an *ab initio* potential energy surface with accuracies of nearly one cm⁻¹, making the isotopic shifts between ¹²CH₄ and ¹³CH₄ a reliable criterion to locate new bands. Thus, the ¹³CH₄ spectrum provided highly valuable information to substantiate tentative vibrational assignments of ¹²CH₄, and in turn, the advanced understanding of the ¹²CH₄ spectrum was applied to the ¹³CH₄ spectrum. This advantage is particularly important because an effective Hamiltonian in the ¹³CH₄ tetradecad cannot be successfully implemented without a prior reliable modeling of the ¹³CH₄ octad (3600 – 4800 cm⁻¹) [1].

Lacking guidance from theoretical models, a complementary and independent insight of the ¹³CH₄ tetradecad structure can be obtained by determining empirical lower state energies using the temperature dependence of the measured line intensities. Independent of any theoretical interpretation, the lower state energy value, $E'' \approx B_0 J''(J''+1)$, and thus the value of the angular momentum J'' , can be deduced from the intensity values of a given transition, $S_{\nu_0}(T)$ and $S_{\nu_0}(T_0)$, observed at two temperatures, T and T_0 . This approach (hereafter called *the two temperature method*) has been successfully applied to methane in natural abundance in a number of studies, including the Margolis studies [9,10] and our recent studies of the ¹²CH₄ tetradecad [13,14] and the icosad near 1.3 μm [15,16]. For example, cold temperature intensities of the ¹²CH₄ tetradecad [14] were combined with the intensity values at room temperature (RT) from a preliminary version of the line list [2] constructed in relation with

the “Greenhouse Gases Observing Satellite” (GOSAT) project. The advantage of the GOSAT line list is that it has a two orders of magnitude smaller intensity cut off compared to HITRAN and GEISA [4,5] line list in the 5500- 6184 cm^{-1} region. A prerequisite of the application of the same method to the $^{13}\text{CH}_4$ isotopologue is the construction of two extensive line lists with accurate intensities at two temperatures. In the present contribution, intensity measurements were performed at room temperature from absorption spectra recorded by Fourier Transform Spectroscopy ($l = 13$ and 73 m) and at 81 K by differential absorption laser spectroscopy ($l = 1.4$ m). By applying the two temperature method, empirical lower state energies could be systematically derived, thus extending the assignments obtained by Nikitin *et al.* [12] on the basis of spectra at 180, 240 K and 298 K with a short optical path (0.0875 m). In Fig. 1, we present an overview comparison of the present line lists at 81 and 296 K compared to the assignments reported by Nikitin *et al.* [12].

In the following sections, we provide the experiment details (Section 2) and describe the construction of the room and cold temperature line lists (Section 3). Then we apply the *two temperature method* (Section 4) to obtain our empirical J values. These results are discussed (Section 5) and compared to known assignments from HITRAN [4] and Nikitin *et al.* [12].

2. EXPERIMENT

The Fourier transform spectrometers (FTS) at the Kitt Peak National Observatory (Tucson, USA) and a the Bruker 125 HR spectrometer at the Jet Propulsion Laboratory (Pasadena, USA) were used to acquire two $^{13}\text{CH}_4$ spectra at room temperature while the differential absorption spectroscopy at Grenoble University (France) provided corresponding data at 81 K. Table 1 provides an overview of the datasets.

Fourier Transform Spectroscopy at room temperature

One spectrum at higher optical density was obtained in 1999 with the FTS located at the McMath-Pierce Solar telescope on Kitt Peak Mountain in Arizona. The intended purpose was to identify weak features in normal sample spectra of the octad [17], but the standard near-IR bandpass for this FTS also included the tetradecad region. The experimental set up was similar to that described in numerous other studies involving the 6-m base multipass cell at Kitt Peak (e. g. CH_4 , CO_2 and CO [18-20]). As indicated in Table 1, an enriched sample of $^{13}\text{CH}_4$ was scanned at 0.0109 cm^{-1} resolution using a 73 m optical path and a pressure value of 0.684 Torr at 295.9 K. The integration time for this scan was one hour.

In 2008, a second absorption spectrum of $^{13}\text{CH}_4$ was taken to characterize the stronger $2\nu_3$ lines. For this, a Bruker IFS-125HR at JPL was configured with a Tungsten lamp source, a CaF_2 beam splitter, and a LN_2 -cooled photovoltaic InSb detector. The nominal aperture diameter was set to 1.3 mm, and an optical interference filter provided a usable bandpass from 5700 to 6500 cm^{-1} . The maximum optical path difference (MOPD) was 90 cm, producing an unapodized spectral resolution of 0.0056 cm^{-1} (0.5/MOPD) [21]. In order to maximize the resolving power, no apodization was applied to the interferograms. The FTS chamber was evacuated to less than 0.012 Torr to minimize residual H_2O and CO_2 absorption.

The Bruker spectrum was obtained with a sample pressure of 0.882 Torr at 293.6 K using 99% enriched $^{13}\text{CH}_4$. From retrieved line intensities, the $^{12}\text{CH}_4$ abundance was later found to be between 0.7% and 0.9%. The sample was held in a multipass cell configured with wedged KCl windows that was set to an optical path of 13.09 m (12 passes) (as determined in a prior study [22]).

No zero-offset was noticed, and the instrument was observed to be stable; no shift or drift in the baseline and frequency was revealed by comparing individual spectra created from 5–10 minute coadding. Consequently, the integration times of six hours achieved peak-to-peak signal-to-noise (SNR) ratios of 1000 without distorting the line shapes. In Fig. 2, overview plots of the Bruker and Kitt Peak FTS spectra of $^{13}\text{CH}_4$ at room temperature are shown.

As described by Sung *et al.* [22], the instrument was well characterized with no significant instrumental line broadening or line shape distortion. This was confirmed using a 2nd cell of HCl placed inside the detector chamber of the FTS in order to simultaneously record the 2 – 0 band at 1.72 μm [4]. These features were utilized to derive the instrumental line shape function, modulation efficiency and residual phase errors using LINEFIT (ver.11) from Hase *et al.* [23]. The modulation efficiency was observed to be better than 0.99 (i.e., 1% degradation) and residual phase errors better than 0.004 radian (corresponding to less than 0.3°) across the maximum optical path difference (MOPD), which are better than expected performance limits (0.96 and 0.01 rad., respectively) as for a nearly perfect ILS [23]. Therefore, the ILS calculated from a *sinc* function with the aperture (field-of-view) corrections was used during spectrum curve fitting to retrieve line parameters [24].

Both FTS spectra were initially intended only for $^{13}\text{CH}_4$ line positions, and thus lower pressures (less than 1 Torr) were used. For the wider bandpass Kitt Peak scan, residual H_2O absorptions appearing between the octad and tetradecad from 5200 to 5400 cm^{-1} provided the frequency standards (previously calibrated [25] against the 2–0 transitions of CO [26]). These

same H₂O features fell outside in the narrower Bruker bandpass so we initially calibrated the 2nd spectrum against the R branch of the 2–0 band of HCl centered at 5667 cm⁻¹. For both spectra, the rms (precision) of observed - standard line centers was 0.00015 cm⁻¹ or better following correction using a multiplying factor. However, detectable systematic offsets of 2.5×10⁻⁴ cm⁻¹ were seen in the calibrated line centers obtained by peak finding from the two sets of FTS spectra. Inspection of earlier literature [27] revealed that the quoted accuracy of the 2–0 HCl lines was only 0.0002 cm⁻¹ and that pressure shifts might contribute as additional uncertainty (up to 0.0001 cm⁻¹)[4]. Rather than attempting to resolve this discrepancy, we simply renormalized the positions from the Bruker spectrum to match the calibrated positions from the Kitt Peak spectrum because the accuracies of the CO standards were a factor of six times better [26]).

Differential absorption spectroscopy at 81 K

The spectra of ¹³CH₄ at 81 K were recorded by differential absorption spectroscopy using a cryogenic cell cooled down to liquid nitrogen temperature and a series of 11 distributed feed back (DFB) fibered laser diodes as light sources. A gas temperature of 81±1 K was determined from the Doppler line broadening [28]. This value is what we refer to as “*liquid nitrogen temperature*” (LNT).

The experimental set up has been described in details in Refs. [14,28]. Briefly, the DFB laser diode was tuned over about 30 cm⁻¹ by a slow temperature scan from -10 to 60 °C within 11 minutes. The series of 11 DFB fibered laser diodes allowed for a continuous coverage of the 5852-6124 cm⁻¹ range, except for an inaccessible gap between 6004.5 and 6005.8 cm⁻¹. The individual spectra were linearized using an etalon signal (1GHz FSR), and calibrated independently by statistically matching the line positions to the values measured by FTS at room temperature (see above). The standard deviation error of the differences between the line positions and FTS values was minimized leading to *rms* values on the order of 1×10⁻³ cm⁻¹. The absorption path length was 142 cm and the gas pressure was continuously measured during the recordings. The methane sample enriched in ¹³C (>99%) was purchased from Isotec, Inc. The whole investigated region was recorded at a pressure of 8.9 Torr (at LNT). As the strong multiplets of the 2v₃ band were saturated at this pressure, additional spectra were recorded with pressure values of 0.34 and 1.3 Torr (as listed in Table 1). Figure 3 shows a comparison of the RT and LNT spectrum where the variation of the relative line intensities is very pronounced.

3. LINE INTENSITY RETRIEVAL

The line intensity, S_{ν_0} (cm/molecule), of a rovibrational transition centred at ν_0 , was obtained from the integrated line absorbance, I_{ν_0} (cm⁻²/molecule):

$$I_{\nu_0}(T) = \int_{line} \alpha_{\nu} l dv = \int_{line} \ln \left[\frac{I_0(\nu)}{I(\nu)} \right] dv = S_{\nu_0}(T) N l \quad (1)$$

where:

$\frac{I_0(\nu)}{I(\nu)}$ is the ratio of the incident intensity to the transmitted intensity,

l is the absorption pathlength in cm,

ν is the wavenumber in cm⁻¹,

$\alpha(\nu)$ is the absorption coefficient in cm⁻¹,

and N is the molecular concentration in molecule/cm³ obtained from the measured pressure value: $P = NkT$.

Separate line lists were created from the retrievals, one for the room temperature data and another from the cold data. The measured intensities were obtained from the different spectra by non-linear least squares curve-fitting techniques, but two different software packages [26,29] were used for the two datasets.

Room temperature spectra

With the FTS data, line centers and absorption depths were first obtained by peak finding of the apodized and interpolated spectrum. These were used to initialize the synthetic spectrum so that positions and intensities could be adjusted to minimize differences between unapodized observed and calculated spectra. Retrievals were done one spectrum at a time. Features not initially detected by peak-finding were added to the fit manually. A Voigt line shape was assumed with the self-broadened widths held fixed to a constant default value (0.09 cm⁻¹/atm). An example of curve fitting with a room temperature scan is shown in Fig. 4 (*left side*).

Several hundred strong features with intensities greater than 4×10^{-23} cm/molecule were generally taken solely from the Bruker FTS spectrum, while all lines weaker than 1×10^{-23} cm/molecule came from the Kitt Peak scan (recorded at 295.9 K). Only the intermediate range intensities were obtained as averages of the retrievals of the two spectra. At the end of the investigation, the room temperature line list was reformed using empirical lower state values derived from the LNT intensities. If a lower state was known (from an assignment or

estimated from the LNT intensities), the intensities were normalized to 296 K; if no lower state energy was available, the intensities of lines were at temperature of the measured spectrum. In all, 3481 features between 5850 and 6150 cm^{-1} were obtained at room temperature with intensities that varied over three orders of magnitude from 3.3×10^{-25} to 1.3×10^{-21} $\text{cm}/\text{molecule}$. The full line list is reported as Supplementary Material and contains the measurements, the known assignments [4,12] with the calculated lower state energy [4] suggested by the empirical values. The resulting line positions from the two spectra often agreed to within 0.0001 cm^{-1} , and this value is thought to be representative of the experimental precision for unblended features well separated from neighboring lines. However, the strongest transitions of the $2\nu_3$ band of $^{13}\text{CH}_4$ often fall together in manifold and so the precisions of those lines can be worse if the overlapping is severe. Finally, as discussed previously, the absolute accuracy may be only $\sim 0.0003 \text{ cm}^{-1}$; the overall wavenumber calibration should be revisited in future studies.

For line intensities, the precisions also depend on such things as the degree of blending, the success of the retrieval process, the size of the absorption relative to the signal to noise ratio etc., while the absolute accuracies depend greatly on how well the experimental gas conditions and optical path lengths are characterized. Initially, it was found that the intensities from two FTS scans were unexpectedly different by $\sim 20\%$; we eventually concluded that the recorded optical density of the Kitt Peak spectrum was wrong; no specific cause was identified. We therefore elected to accept the observed intensities from the Bruker spectrum because it was recorded with close attention to sample purity and stability, and the use of calibrated pressure gauges previously validated by an earlier OCS study [22]. The intensities of the Kitt Peak spectrum were then adjusted by a factor of 0.8 and used with the 81 K data to determine lower state energies. This choice was later validated by comparing the derived values for assigned transitions [12]. The precisions of the isolated features are thought to be better than 3%. However, the very weakest features measured in the Kitt Peak spectrum are retained in the line list, but their accuracies may be no better than 0.010 cm^{-1} for positions and up to $\pm 200\%$ for the intensities. In fact, a few of the weakest lines may be spurious.

Low temperature spectra

Contrary to our previous analysis [13-16], in the present study we took advantage of the availability of spectra recorded at several pressures at 81 K to apply a multispectrum fitting treatment and improve the retrieval of the spectroscopic parameters [29]. The first step of the analysis was to identify the spectral sections of overlapping or nearby transitions that could be treated independently. For each independent spectral section, the local baseline was assumed to be a quadratic function of the wavenumber. Spectral lines were fitted with a Voigt function profile with the HWHM of the Gaussian component fixed to its theoretical value. The experimental points with absorption larger than 80% were excluded from the fit. Apart from the local baseline, line positions, line intensities and self-broadening coefficients were obtained from the simultaneous fit of the experimental spectra. The DFB line width (1-5 MHz) is much smaller than the full Doppler broadening at LNT [~ 300 MHz (FWHM)] and thus was neglected. An example of intensity retrieval with the cold data is shown in Fig. 4 (*right side*). We note that the narrowing of the Doppler width by a factor of two in the LNT spectra improves the experimental resolution sufficiently to resolve some otherwise blended $2\nu_3$ manifolds.

The simultaneous fit of two spectra reveals that the adopted Voigt profile leads to systematic deviations; this is also true for the room temperature spectrum (Fig. 4 *left side*). While such differences in the cold data might be due to the temperature gradient in the small sections of the cryogenic cell lying between the ends of the cold jacket and the cell windows, it seems more likely that a more sophisticated line shape profile is needed [30, 31]. As a test, retrieval with cold data was performed using a Rautian profile; this led to better fitting residuals that altered the line intensity values by less than 1.5 %. This value can be considered as a rough estimation of the fitting error related to the choice of the line profile.

One interesting result of multispectrum retrieval is that some self broadening coefficients could be reliably determined at 81 K despite the low pressures (up to 9 Torr). We obtained an averaged width of $0.23 \text{ cm}^{-1}/\text{atm}$, at 81 K, in very good agreement with an extrapolation of the values obtained down to 100 K from the depopulation rate of the $V_3=2$ population levels [32].

From these retrievals, two separate line lists at 81 K and 296 K were compiled for the upper region of the $^{13}\text{CH}_4$ tetradecad. As seen in Table 2, the final line list near 296 K consisted of 3396 lines of $^{13}\text{CH}_4$ and 85 lines of $^{12}\text{CH}_4$ with intensity values ranging from 3.3×10^{-25} to 1.3×10^{-21} cm/molecule, while the final line list at 81 K consisted of 1629 lines with intensities between 2.9×10^{-26} to 3.8×10^{-21} cm/molecule. The next step of the analysis was

to combine these empirical data in order to estimate lower state energies of the observed features.

4. DETERMINATION OF THE LOWER STATE ENERGY

Taking into account the partition function, the lower energy can be calculated from the following equation (see Ref. [11] for more details):

$$\ln\left(\frac{S_{v_0}(T)T^{3/2}}{S_{v_0}(T_0)T_0^{3/2}}\right) = E\left[\frac{1}{kT_0} - \frac{1}{kT}\right] \quad (2)$$

where T_0 and T are the RT and the LNT, respectively.

The coincidence of the line centers was used as the criterion to associate transitions in the RT and LNT line lists. Consequently, the results depend on the quality of the wavenumber calibration of the spectra and the precision on the measured line centers. As a first step, we considered as identical RT and LNT transitions when the difference, δ , of their line centres was less than 0.002 cm^{-1} . This value corresponded to one fifth and tenth of the Doppler width (FWHM) at LNT and RT, respectively. With this criterion, 983 RT lines were matched. A careful examination of the line lists and spectra revealed that the $\delta < 0.002 \text{ cm}^{-1}$ criterion was too strict because any features had poorer precisions if they were blended or very weak. This degradation also occurred frequently in the icosad region at $1.3 \text{ }\mu\text{m}$, as discussed extensively in Ref. [16].

We undertook a careful line-by-line examination of the spectra and line lists in order to associate the maximum number of identical transitions without increasing the number of accidental coincidences. With a wider criterion of $0.002 < \delta < 0.005 \text{ cm}^{-1}$, 213 other lines were matched which increased by 9% the total absorbance at LNT and RT. The total of 1196 matches displayed on Fig. 1 represents 99.2 and 84.6 % of the total absorbance at 81 and 296 K respectively. Nevertheless, about 65 % of the transitions measured at RT remain without LNT partners. This occurs mainly because a high number of RT lines are high J transitions which vanish in the LNT spectrum. For example, the intensity of a transition from a $J = 11$ level is decreased by three orders of magnitude when cooling from 296 K to 81 K.

Using Eq. (2), the lower state energy values, E'' , were empirically determined and the corresponding J values were calculated as the positive root of the $E = B_0J(J+1)$ equation (with $B_0 = 5.241 \text{ cm}^{-1}$). As an example, the obtained J values have been indicated on the RT and LNT spectra displayed previously in Fig. 3. The reliability of the derived lower state energies is confirmed by comparing the results for known assignments. The first example is given in

Table 3, which shows the measured values for the strong P(6) manifold of $2\nu_3$. The columns, from left to the right, represent the cold position, the cold and room temperature intensities, the empirical lower state energy computed from Eq. (2) using the present measured intensities, the theoretical value [4] based on the accepted quantum assignment, the corresponding experimental lower state J'' and the lower state quantum numbers (J'', C, n) of the assignment. For this manifold, the agreement of the deduced and known J'' values is excellent. As seen in **Table 3**, the precision is demonstrated because the cold and room temperature intensities for allowed A, F, E transitions are close to the expected ratios of 5:3:2. In addition, line intensities are similar for the four allowed F lines and also for the A pair. The absolute accuracy is seen to be sufficient because the correct J'' is obtained for all six allowed lines. There is even the detection of a weak feature which may later be confirmed by theory to be a forbidden line associated with a $J' = 5$ F2 upper state level.

For a second validation, we note that 67 % of the experimental J'' values fall within ± 0.25 of an integer value. As seen in the histogram shown in **Fig. 5**, the propensity of the J values to be close to integer values is a clear indication of the validity of the method. Nevertheless, the histogram shows that the quality of the J determination degrades both for the $J = 0-2$ values (which correspond, respectively, to $E'' = 0, 10,$ and 31 cm^{-1}) and for the higher J values (> 9) which correspond to the weakest transitions in the RT and LNT spectra, respectively.

Finally, the third validation comes from the very good agreement with 248 assignments reported in the isotopic shifts analysis by Nikitin *et al.* [12]. As seen in **Fig. 6**, 222 of our rounded J values coincide exactly while a difference of only ± 1 is found for 19 transitions.

5. DISCUSSION

In **Fig. 7**, we plot the full E'' dataset as a function of the derived J values to show the distribution of the RT and LNT line intensities, together with the associated histograms. The marked dissymmetry of the RT and LNT panels reflects the considerable intensity variation of the transitions corresponding to the low and high J values. The contrast between integer and non integer J values is even more evident when magnitude of line intensities is considered; the intensities uncertainties are worse for weaker lines and thus results in more non integer J values. Nevertheless, transitions that do fall close to integer J values represent, respectively, 86.5 and 89.9 % of the total absorbance at 81 and 296 K.

In future studies, the new intensity and experimental J'' values can be used to determine the rotational and then vibrational quantum assignments. For example, in **Fig. 8** are

shown the experimental line positions vs the rounded values of J'' up to $J''=5$, plotted as open circles. In order to use line intensities as an additional criterion, intensities at 81 K were divided by the quantity $(2J''+1) \exp(-E''/kT)$ and ranked in three groups represented by the size and color of the circles: large **black**, medium **blue** and small **red** corresponding to strong, medium and weak transitions. In addition, some known quantum assignments from Nikitin *et al.* [12] are included in Fig. 8 for four sub-vibrational states with the vibrational identity indicated by the color of the solid circles, as listed in the legend. Also indicated on the figure are all the individual vibrational symmetries of upper tetradecad. The $2\nu_3$ F2 component near 5988 cm^{-1} gives rise to regular P , Q and R structure with $P(J)$, $Q(J)$ and $R(J)$ transitions split into several tetrahedral components. Inspection of Fig. 8 reveals that its transitions form the signature pattern by which bands can be located; the successive low J values fall in straight lines that are easily recognized as R (positive slope), Q (horizontal line) and P (negative slope) branches. One immediately sees a similar pattern involving medium intensity lines (**blue** circles) around 5850 cm^{-1} . The most likely assignment is $\nu_1 + \nu_3$, predicted to lie at 5851 cm^{-1} (see Table 1 of Nikitin *et al.* [12]) The other states between 5860 and 5900 cm^{-1} all belong to $3\nu_2 + \nu_4$ and are likely to account for observed weak lines plotted with small **red** circles. Of course, a good theoretical analysis of both positions and intensities must be performed [2] to confirm candidate assignments, but the present results provide the wealth of new data (~ 1200 J values) to interpret the upper tetradecad of $^{13}\text{CH}_4$.

It is worth noting that the number of transitions observed at LNT is almost half of that measured at RT. However, the LNT line list also includes 400 additional transitions not detected in our current selection of RT spectra, and many obviously correspond to very low J values (0-4). Using wider matching criterion might produce some more effective J'' in the case of blended bundles of lines. A theoretical prediction with reasonable calculated intensities would be needed to eliminate accidental coincidences. Future efforts in this region should also include the use of room and cold temperature spectra recorded with a wider range of optical densities and temperatures.

As mentioned in the introduction, early measurements of Q_1 , R_0 and R_1 suggested that there was an isotopic dependence in the $2\nu_3$ line intensities [7,11]. This question is reconsidered in Table 4 where ratio values are computed using RT measurements from Fox *et al.* [7], Margolis [9], and the present work [TW]. One recent R_0 measurement at 296 K from Hurtsmans *et al.* [33] is shown for accuracy validation. The individual 30-year-old measurements [7] are quite different from the recent intensities at room temperature, and the

ratios are smaller; 1.089 (5) rather than the 1.33 (5) reported by Fox *et al.* [7]. This provides some validation of the measurement precisions, but not the absolute accuracies of the $^{13}\text{CH}_4$ room temperature intensities. The 3% accuracies claimed by Margolis [9] have been somewhat confirmed by Hurtsmans *et al.* [33] and Boussin *et al.* [34]. However, the present $^{13}\text{CH}_4$ values for strong lines at room temperature are based on only one spectrum. Additional measurements are needed to characterize those absolute accuracies. Until this is done, no precise conclusion can be reached about isotopic dependences for $2\nu_3$ line intensities.

Methane was detected in the major planets 76 years ago [35] and is now considered ubiquitous in the universe, existing in many different gaseous environments with temperatures that can range from 50 K to perhaps 3000 K (in exosolar planets). Remote sensing of these bodies requires a comprehensive collection of molecular line parameters for its three most abundant isotopologues. For instance, the $^{12}\text{CH}_4$ and $^{13}\text{CH}_4$ infrared absorptions observed in the spectra of Titan recorded by the Cassini Composite Infrared Spectrometer (CIRS) were recently used to determine the $^{12}\text{C}/^{13}\text{C}$ isotopic ratio in Titan's stratosphere [36]. Previously, quantum mechanical analyses of near-IR methane were almost intractable, and the public databases [4,5] could not collect complete information; this hindered efforts to monitor methane concentrations even in the Earth's troposphere [37]. For the upper tetradecad of $^{13}\text{CH}_4$, the databases had only 83 transitions of the strongest band ($2\nu_3$) primarily because some transitions were blended or even masked by $^{12}\text{CH}_4$ lines. In addition, so little analysis was done previously that weaker $^{13}\text{CH}_4$ features already measured in normal sample spectra could not be identified as isotopic lines. As an example of the improvements, two $2\nu_3$ multiplets observed at RT and LNT are compared in Fig. 9 to the HITRAN values. Overall, the structure of the multiplets as obtained from fitting of the FTS spectrum is in very good agreement with the spectrum recorded at 81 K. Thus, important discrepancies in the $^{13}\text{CH}_4$ parameters on HITRAN can be corrected with our RT line list, providing a significant improvement both in terms of accuracy and completeness.

We provide as Supplementary Material two complete line lists of transitions, one measured at 81 K (1629 transitions) and the other at 296 K (3481 transitions). Part of the information from these line lists is shown in Table 5. For the 1196 pairs of associated transitions, the E and J values of the lower state are provided. As larger uncertainties on the line intensities are expected for the transitions showing larger difference between their RT and LNT centers, we have specifically marked the J values obtained from transitions with $0.002 < \delta < 0.005 \text{ cm}^{-1}$ which are believed to be less accurate.

6. CONCLUSION

This study reports extensive measurements of positions and intensities of $^{13}\text{CH}_4$ from 5850 to 6150 cm^{-1} . Past attempts in theoretical analyses of this region have made little progress partly because quantum assignments could not be easily discerned. Obtaining empirical lower state energies for about 1200 transitions and detection of an additional 400 features at 81 K thus removes a major obstacle at a time when new theoretical efforts [2,12] are being undertaken to model the tetradecad of both methane isotopologues. The line lists provided as Supplementary Material do precisely account for the temperature dependence of 90 % of the total integrated $^{13}\text{CH}_4$ absorption in this region. These exhaustive lists of nearly 3500 features at room temperature can thus serve as an interim database for laboratory studies and remote sensing applications. We remind that the current $^{13}\text{CH}_4$ data for this region are the 83 transitions in the HITRAN database and the 198 newly assigned transitions from Ref. [12].

A possible extension of this work could be performed by combining the results obtained for the $^{13}\text{CH}_4$ and $^{12}\text{CH}_4$ tetradecad. Using the same method based on the isotopic shifts as presented in Ref. [12], the line by line correspondence of the $^{13}\text{CH}_4$ and $^{12}\text{CH}_4$ transitions should help to vibrationally assign the different bands, for both isotopologues. This information associated to the empirical J values determined for the two isotopologues [14] will help to achieve a global theoretical interpretation of the tetradecad.

Future experimental efforts are still needed to understand the whole of tetradecad structure, however. The weaker lines must be characterized from 4750 to 6250 cm^{-1} by using larger optical paths at room and at a range of cold temperatures to discern a wider range of J values. Here we applied a multispectrum fitting technique only to the 81 K spectra recorded at several pressures while the spectroscopic parameters at 296 K were retrieved independently. In some future effort, the multispectrum treatment of both the 81 K and 296 K spectra simultaneously could solve for E'' directly. Indeed, the decrease by a factor of two of the Doppler broadening by cooling down to 81 K spectra is highly valuable to resolve strongly blended multiplets as those of the $2\nu_3$ band. However, we are mindful that with very high optical density spectra, the retrieval process must be initiated with a reasonable theoretical prediction of the spectra. In the past, methane investigators have often analyzed positions and quantum assignments aided by some initial intensities in a *preliminary* analysis, which in turn enables a more thorough interpretation of the very complex region. The present study is one important step toward this ultimate goal.

Acknowledgements

O.M. L. (IAO, Tomsk) is grateful to the French Embassy in Moscow for a two months visiting support at Grenoble University. This work is part of the ANR project “CH4@Titan” (ref: BLAN08-2_321467). The supports by RFBR (Grant RFBR 09-05-92508-ИК_a), CRDF (grant RUG1-2954-TO-09) and by the Groupement de Recherche International SAMIA between CNRS (France), RFBR (N 09-05-93105, Russia) and CAS (China) is acknowledged. . Part of the research described in this paper was performed at the Jet Propulsion Laboratory, California Institute of Technology, under contract with the National Aeronautics and Space Administration.

References

- [1] S. Albert, S. Bauerecker, V. Boudon, L. R. Brown, J. P. Champion, M. Loëte, and A. Nikitin, M. Quack, *Chem. Phys.* 356 (2009) 131–146.
- [2] A.V. Nikitin, O.M. Lyulin, S. N. Mikhailenko, V. I. Perevalov, N.N. Filippov, I.M. Grigoriev, I. Morino, T. Yokota, R. Kumazawa and T. Watanabe, *in preparation*.
- [3] H. M. Niederer, S. Albert, S. Bauerecker, V. Boudon, J. P. Champion and M. Quack, *Chemia* 62 (2008) 273–276.
- [4] L. S. Rothman, I. E. Gordon, A. Barbe, D. Chris Benner, P. F. Bernath, M. Birk, V. Boudon, L. R. Brown, A. Campargue, J.-P. Champion, K. Chance, L. H. Coudert, V. Dana, V. M. Devi, S. Fally, J.-M. Flaud, R. R. Gamache, A. Goldman, D. Jacquemart, I. Kleiner, N. Lacome, W. J. Lafferty, J.-Y. Mandin, S. T. Massie, S. N. Mikhailenko, C. E. Miller, N. Moazzen-Ahmadi, O. V. Naumenko, A. V. Nikitin, J. Orphal, V. I. Perevalov, A. Perrin, A. Predoi-Cross, C. P. Rinsland, M. Rotger, M. Šimečková, M. A. H. Smith, K. Sung, S. A. Tashkun, J. Tennyson, R. A. Toth, A. C. Vandaele and J. Vander Auwera, *J. Quant. Spectrosc. Radiat. Transfer* 110 (2009) 533–572.
- [5] N. Jacquinet-Husson, N.A. Scott, A. Chédin, L. Crépeau, R. Armante, V. Capelle, J. Orphal, A. Coustenis, A. Barbe, M. Birk, L. R. Brown, C. Camy-Peyret, C. Claveau, K. Chance, N. Christidis, C. Clerbaux, P.F. Coheur, V. Dana, L. Daumont, M.R. Debacker-Barilly, G. Di Lonardo, J.M. Flaud, A. Goldman, A. Hamdouni, M. Hess, M. D. Hurleyo, D. Jacquemart, I. Kleiner, P. Köpke, J. Y. Mandin, S. Massie, S. Mikhailenko, V. Nemtchinov, A. Nikitin, D. Newnham, A. Perrin, V. I. Perevalov, S. Pinnocki, L. Régalia-Jarlot, C. P. Rinsland, A. Rublev, F. Schreier, L. Schult, K. M. Smith, S. A. Tashkun, J. L. Teffo, R. A. Toth, Vl. G. Tyuterev, J. Vander Auwera, P. Varanasi and G. Wagner, *J. Quant. Spectrosc. Radiat. Transfer* 109 (2008) 1043–1059.
- [6] L. S. Rothman, R. R. Gamache, A. Goldman, L. R. Brown, R. A. Toth, H. M. Pickett, R. L. Poynter, J. M. Flaud, C. Camy-Peyret, A. Barbe, N. Husson, C. P. Rinsland and M. A. H. Smith, *Appl. Opt.* 26 (1987) 4058–4097.
- [7] K. Fox, G. W. Halsey, S. J. Daunt, W. E. Blass and D. E. Jennings, *J. Chem. Phys.* 72 (1980) 4657–4658.
- [8] K. Fox, G. W. Halsey and D. E. Jennings, *J. Mol. Spectrosc.* 83 (1980) 213–222.
- [9] J. S. Margolis, *Appl. Opt.* 27 (1988) 4038–4051.
- [10] J. S. Margolis, *Appl. Opt.* 29 (1990) 2295–2302.
- [11] P. Varanasi, *J. Quant. Spectrosc. Radiat. Transfer* 25 (1981) 319–323.
- [12] A.V. Nikitin, S. Mikhailenko, I. Morino, T. Yokota, R. Kumazawa and T. Watanabe, *J. Quant. Spectrosc. Radiat. Transfer* 110 (2009) 964–973.
- [13] B. Gao, S. Kassi, A. Campargue, *J. Mol. Spectrosc.* 253 (2009) 55–63.

- [14] L. Wang, S. Kassi and A. Campargue, *J. Quant. Spectrosc. Radiat. Transfer* (*in press*) doi:10.1016/j.jqsrt.2009.10.019.
- [15] E. Sciamma-O'Brien, S. Kassi, B. Gao and A. Campargue, *J. Quant. Spectrosc. Radiat. Transfer* 110 (2009) 951–963.
- [16] A. Campargue, L. Wang, S. Kassi, M. Mašát and O. Votava, *J. Quant. Spectrosc. Radiat. Transfer* (*in press*) doi:10.1016/j.jqsrt.2009.11.025.
- [17] J. C. Hilico, O. Robert, M. Loete, S. Toumi, A. S. Pine and L. R. Brown, *J. Mol. Spectrosc.* 208 (2001) 1–13.
- [18] L. R. Brown, *J. Quant. Spectrosc. Radiat. Transfer* 96 (2005) 251–270.
- [19] R. A. Toth, L. R. Brown, C.E. Miller, V. M. Devi, D. C. Benner and M. Dulick, *J. Mol. Spectrosc.* 239 (2006) 221–242.
- [20] C. Chackerian, R. Freedman, L.P. Giver, L.R. Brown, *J. Mol. Spectrosc.* 210 (2001) 119–126.
- [21] R. S. Booth, J. W. Brault and A. Labeyrie. *High resolution in Astronomy*. (Geneva Observatory, CH-1290 Sauverny, Switzerland, 1985), 1–61.
- [22] K. Sung, R. A. Toth, L. R. Brown and T. J. Crawford, *J. Quant. Spectrosc. Radiat. Transfer* 110 (2009) 2082–2101.
- [23] F. Hase, T. Blumenstock and C. Paton-Walsh, *Appl. Opt.* 38 (1999) 3417–3422.
- [24] L. R. Brown, J. S. Margolis, R. H. Norton and B. Stedry, *Appl. Spectrosc.* 37 (1983) 287–292.
- [25] L. R. Brown and J. S. Margolis, *J. Quant. Spectrosc. Radiat. Transfer* 56 (1996) 283–294.
- [26] C. R. Pollock, F. R. Petersen, D. A. Jennings, J. S. Wells, and A. S. Maki, *J. Mol. Spectrosc.* 99 (1983) 357–368.
- [27] R. B. Le Blanc, J. B. White and P. F. Bernath, *J. Mol. Spectrosc.* 164 (1994) 574–579.
- [28] S. Kassi, B. Gao, D. Romanini and A. Campargue, *Phys. Chem. Chem. Phys.* 10 (2008) 4410–4419.
- [29] D. Jacquemart, J. Y. Mandin, V. Dana, N. Picqué and G. Guelachvili, *Eur. Phys. J. D.* 14 (2001) 55–69.
- [30] D. Mondelain, C. Camy-Peyret, W. Deng, S. Payan and A. W. Mantz, *Appl. Phys. B90* (2008) 227–233.
- [31] H. Tran, J.-M. Hartmann, G. Toon, L. R. Brown, C. Frankenberg, T. Warneke, P. Spietz and F. Hase *J. Quant. Spectrosc. Radiat. submitted.*

- [32] F. Ménard-Bourcin, J. Ménard and C. Boursier, *J. Mol. Spectrosc.* 242 (2007) 55-63.
- [33] D. Hurtmans, G. Dufour, W. Bell, A. Henry, A. Valentin and C. Camy-Peyret, *J. Mol. Spectrosc.* 215(2002) 128–133. doi:10.1006/jmsp.2002.8620.
- [34] C. Boussin, L. Regalia, J.-J. Plateaux and A. Barbe, *J. Mol. Spectrosc.* 191 (1998) 381–383.
- [35] A. Adel and V. M. Slipher, *Phys. Rev.* 46 (1934) 0240-0241.
- [36] C.A. Nixon, R.K.Achterberg, S.Vinatier, B.Bézar, A. Coustenis, P.G.J. Irwin, N.A. Teanby, R. de Kok, P.N. Romani, D.E.Jennings, G.L.Bjoraker and F.M.Flasar, *Icarus* 195 (2008) 778–791
- [37] R. A. Washenfelder, P. O. Wennberg and G. C. Toon, *Geo. Res. Lett.* 30 (2003) 2226–2003. doi: 10.1029/2003GL017969.

Figure Captions

Fig. 1. Overview of $^{13}\text{CH}_4$ measurements between 5850 and 6150 cm^{-1} :

Upper panel: 3481 intensities at 296 K obtained from two FTS spectra (*this work*);

Middle panel: 267 transitions at 180 K assigned for $\nu_2+\nu_3+\nu_4$, $2\nu_2+\nu_3$ and $2\nu_3$ from Ref. [12];

Lower panel: 1629 intensities derived at 81 K by differential absorption spectroscopy (*this work*).

The full circles (*in blue*) highlight the 1196 pairs of transitions observed at 81 and 296 K, for which the lower energy values could be derived (*see section 4 in the text*).

Fig. 2. The room temperature spectrum of $^{13}\text{CH}_4$ between 5800 and 6200 cm^{-1} recorded with the JPL Bruker 125 (*left*) and the Kitt Peak FTS (*right*); the experimental details are summarized in [Table 1](#).

Fig. 3. Comparison of the $^{13}\text{CH}_4$ at 293.6 K (*upper panel*) and 81 K (*lower panel*) to show the dramatic variation of the line intensities. The RT and LNT spectra were recorded at a pressure of 0.885 Torr and 8.9 Torr, respectively. The empirical lower state energies are represented by the observed J values using $E'' \approx B_0 J''(J''+1)$. Note that vibrational assignments were indicated [12] for only two of these features ($J'' = 8$ of $2\nu_2+\nu_3$).

Fig. 4. Examples of the retrieval process with the P(6) manifold of $2\nu_3$ of $^{13}\text{CH}_4$ at room temperature (*left panel*) and 81 K (*right panel*). In both cases the residuals are larger than the signal to noise ratios, suggesting that non-Voigt line shapes might be required.

Left: The RT Bruker spectrum was retrieved one spectrum at a time [24]. In the lower panel, the observed (*in black*) and synthetic (*in red*) spectra are overlaid, and the residuals are shown in the upper panel.

Right: Multispectrum fitting [29] was applied to two LNT spectra for pressures of 1.29 (*red*) and 8.93 (*black*) Torr at 81 K. The two residuals are presented above in corresponding colors.

Fig. 5. Histogram of the empirical J values (*step interval of 0.2*) obtained for $^{13}\text{CH}_4$ between 5852 and 6124 cm^{-1} .

Fig. 6. Comparison of present empirical J values with known $^{13}\text{CH}_4$ assignments of $\nu_2+\nu_3+\nu_4$, $2\nu_2+\nu_3$ and $2\nu_3$ from Ref. [12]. Only 7 rounded values of J_{emp} out of 248 are different by more than one. It should be noted that such differences can indicate that a measured intensity is wrong or that the assigned transition is coincident with a second (*unknown*) transition having a different value of J .

Fig. 7. Line intensities of $^{13}\text{CH}_4$ as a function of the derived empirical lower J values.

Upper panels: The line intensities of $^{13}\text{CH}_4$ between 5852 and 6124 cm^{-1} at 296 K (*left side*) and 81 K (*right side*).

Lower panels: Sums of line intensities corresponding to each step interval of 0.5. Note that 67% of the J values fall within the ± 0.25 of an integer value (*see Fig. 5*), and these corresponds to 89.9 % and 86.5 % of the total absorbance at 296 K and 81 K, respectively.

Fig. 8. The observed $^{13}\text{CH}_4$ line positions vs integer values of the empirical J'' . The open circles are the measurements. The size of the plot symbol indicates the relative intensity of the plotted line (strong, medium, weak corresponds to large, medium small). The known quantum assignments are indicated by the solid dots with colors indicated by the legend. At left are the symmetries of sub-vibrational levels for the upper tetradecad (see text). The F2 state predicted at 5851 cm^{-1} is $\nu_1 + \nu_3$ [12].

Fig. 9. Comparison of the LNT transmission spectrum at 81 K (lower panel) with intensities at 296 K from the present RT line list (middle panel) and the HITRAN database [4] (upper panel). Two $^{13}\text{CH}_4$ manifolds of $2\nu_3$ [Q8 (*left*) and R5 (*right*)] are shown with the empirical lower state J'' values printed above each transition. Note that the feature near 5982.9 cm^{-1} in the LNT scan does not appear in our Bruker FTS scan taken at 293.6 K. The pressure of the LNT spectra was 8.9 and 1.3 Torr, for the left and right panels, respectively.

Table 1 Summary of experimental conditions

	Kitt Peak FTS	JPL Bruker125HR	Diff. Abs.
Light Source	Quartz-halogen	Tungsten lamp	DFB laser diode
Beam Splitter	CaF ₂	CaF ₂	na
Detector	InSb	InSb	InGaAs
Resolution (unapodized) (cm ⁻¹)	0.0109	0.0056	Doppler limited
Sample pressure (Torr)	0.684	0.882	0.34, 1.3, 8.9
Gas sample	¹³ CH ₄ (¹³ C, >90%)	(HCl = 3.84 Torr) ⁺ ¹³ CH ₄ (¹³ C, >99%)	¹³ CH ₄ (¹³ C, >99%)
Path length (m)	73.0	13.09 (HCl = 0.10)	1.42
Temperature (K)	295.9	293.6	81
Useable Band pass (cm ⁻¹)	3600 – 6900	5700 – 6500	5852-6124
Calibration standards	H ₂ O at 1.9 μm [25]	HCl at 1.73 μm [4,25]	Kitt Peak FTS
Calibration factor using stands.	0.999998123(33)	1.0000001410(120) ⁺⁺	
Final calibration factor applied	0.999998123(33)	1.0000001013(12) ⁺⁺	

⁺ HCl was recorded simultaneously to validate performance and instrumental line shape of the FTS.

⁺⁺ Positions were normalized to the Kitt Peak calibration rather than from the HCl positions (see Text).

Table 2 Overview of $^{13}\text{CH}_4$ results and summations

	Room temperature	81 K
Positions in cm^{-1}	5850 \rightarrow 6150 cm^{-1}	5852 \rightarrow 6124 cm^{-1}
⁺ Position Precisions in cm^{-1}	0.0001 \rightarrow 0.0100	0.001 cm^{-1}
Intensities in $\text{cm}/\text{molecule}$	4×10^{-25} to 1.3×10^{-21}	2.9×10^{-26} to 3.8×10^{-21}
⁺⁺ Sum of intensities in $\text{cm}/\text{molecule}$	7.81×10^{-20}	7.43×10^{-20}
⁺ Intensity Precisions	$\pm 1\% \rightarrow \pm 200\%$	$\pm 3\% \rightarrow \pm 50\%$
Number of lines	3481 ⁺⁺	1629
Number of empirical E''		1196

Notes

⁺ Precisions are best for unblended lines with intensities $> 4 \times 10^{-24}$ $\text{cm}/\text{molecule}$ separated by 10 Doppler widths from other nearby features; worst precisions occur for lines closer together than 3 Doppler widths to other features or all lines with intensities smaller than 4×10^{-24} $\text{cm}/\text{molecule}$.

⁺⁺ Absorptions known to coincide with $^{12}\text{CH}_4$ transitions are included because they may arise partly from $^{13}\text{CH}_4$ as well.

Table 3. Sample of $^{13}\text{CH}_4$ measurements for the assigned P6 manifold of $2\nu_3$

Position (cm^{-1})	Intensity ($\text{cm}/\text{mol}\times 10^{-22}$)		E''		J''_{emp}	$J'' \ C'' \ n \ [4]$
	81 K	296 K	Meas.	Calc. [4]		
5920.7049	0.00350					
5920.7920	0.00237	0.0354	358.203		7.80	
5920.8452	0.829	2.14	224.070	219.9237	6.06	6 E 1
5920.8589	1.21	3.12	224.106	219.9253	6.06	6 F2 1
5920.9061	2.01	5.18	224.331	219.9301	6.06	6 A2 1
5920.9411		0.023				
5921.0276	1.18	3.03	223.894	219.9470	6.06	6 F2 2
5921.0475	0.0229	0.0518	213.974	219.9250	5.91	6 F2 1 *
5921.0687	1.18	3.02	225.552	219.9515	6.08	6 F1 1
5921.1045	1.93	5.04	226.020	219.9555	6.09	6 A1 1

* this is likely a forbidden line to same upper state as the prior transition because it falls within 0.002 cm^{-1} of the position predicted from the allowed F2 2 position.

Table 4. Intensity ratios ($^{12}\text{CH}_4 / ^{13}\text{CH}_4$) for Q_1 , R_0 and R_1 of $2\nu_3$

Assignment	Position cm^{-1}	Isotope	Line intensities ($\text{cm}/\text{molecule}$) $\times 10^{22}$		
			Hurtsmans <i>et al.</i> [33]	Fox <i>et al.</i> [7]	Present [9,TW]
Q_1	6004.863	12		2.69	3.23
	5987.218	13		1.92	2.96
		ratio		1.40	1.09
R_0	6015.664	12	5.83	5.11	5.80
	5997.960	13		3.93	5.35
		ratio		1.30	1.08
R_1	6026.227	12		5.15	5.69
	6008.465	13		4.02	5.22
		ratio		1.28	1.09

Notes:

$^{12}\text{CH}_4$ intensities are in natural abundance near 296 K (Margolis [9], Fox *et al.* [7] and Hurtsmans *et al.* [33]); in the present work [TW], the intensities at 296 K are taken from enriched samples at $\sim 99\%$ $^{13}\text{CH}_4$.

Table 5. Sample of information on deposit in the Supplementary Material⁺

<i>T</i> = 81 K		<i>T</i> = 296 K		<i>E</i> (<i>cm</i> ⁻¹)	<i>J</i> _{emp}
<i>Line center</i> (<i>cm</i> ⁻¹)	<i>Line intensity</i> (<i>cm</i> / <i>mol</i>)	<i>Line center</i> (<i>cm</i> ⁻¹)	<i>Line intensity</i> (<i>cm</i> / <i>mol</i>)		
5982.6876	2.70E-25	5982.6861	1.35E-23	453.737	8.82
5982.6996	3.79E-25	5982.6978	5.61E-23	537.950	9.64
5982.7546	5.26E-24	5982.7554	1.50E-23	231.783	6.17
5982.7779	1.94E-25	5982.7766	3.32E-23	549.318	9.75
5982.8326	1.98E-24	5982.8319	8.91E-23	445.744	8.74
5982.8561	1.48E-24	5982.8515	4.37E-24	234.551	6.21*
5982.9054	9.76E-25				
5982.9421	2.78E-24	5982.9417	1.42E-22	455.805	8.84
5982.9976	1.34E-23	5982.9976	2.75E-22	384.980	8.09
5983.0236	8.92E-24	5983.0235	1.80E-22	383.432	8.07
5983.1321	1.25E-23	5983.1319	2.49E-22	382.666	8.06
5983.1471	5.75E-25	5983.1473	4.80E-23	493.601	9.22
5983.2033	1.22E-23	5983.2034	2.47E-22	383.857	8.07
5983.3157	7.96E-26	5983.3144	1.26E-23	543.473	9.70
5983.3247	1.76E-25				
5983.3931	1.58E-25	5983.3949	9.33E-24	466.733	8.95
5983.4948	1.49E-25	5983.4939	2.58E-24	371.788	7.94
5983.5521	1.85E-25				
5983.6191	1.84E-23	5983.6178	2.96E-22	366.038	7.87
5983.6317	2.16E-23	5983.6333	2.46E-22	339.085	7.56
5983.6974	1.26E-24	5983.6972	1.02E-23	312.881	7.24
5983.8393	3.79E-24	5983.8408	4.08E-24	156.336	4.98
5983.8702	1.23E-24	5983.8691	5.49E-24	266.545	6.65
5983.8884	1.21E-24				
5983.9505	5.32E-23	5983.9504	3.63E-22	299.602	7.08
5984.0165	3.49E-23	5984.0165	2.41E-22	300.588	7.09
5984.0501	5.11E-23	5984.0499	3.53E-22	300.410	7.09
5984.1047	8.40E-23	5984.1047	5.74E-22	299.613	7.08
5984.3436	9.45E-25				
5984.3802	4.75E-23	5984.3804	3.27E-22	300.287	7.09
5984.3986	4.79E-23	5984.3988	3.28E-22	299.752	7.08
5984.5832	1.02E-24				
5984.7331	3.15E-24	5984.7347	1.41E-23	266.702	6.65
5984.7586	1.81E-24				
5984.7982	2.93E-22	5984.7981	7.14E-22	219.735	5.99
5984.8353	1.76E-22	5984.8353	4.53E-22	223.863	6.05
5984.8736	1.72E-22	5984.8736	4.47E-22	224.672	6.07
5984.9817	2.12E-22	5984.9796	4.78E-24	392.076	8.16*
5985.0297	2.00E-25	5985.0304	5.42E-24	406.417	8.32
5985.0779	2.74E-22	5985.0780	7.10E-22	224.493	6.06
5985.1097	1.64E-22	5985.1098	4.26E-22	224.638	6.07
5985.1220	1.09E-22	5985.1222	2.80E-22	223.910	6.06

⁺ Measured line centers and line strengths of the methane transitions recorded at 81 K and 296 K near 5983 *cm*⁻¹. Most of the lower state energies, *E*"', and empirical *J*"' values, *J*_{emp}, were obtained for the transitions whose centers coincide within 0.002 *cm*⁻¹. The "*" symbol in the last column marks the lines whose line centers measured in the 81 K and 296 K spectra, differ by 0.002 < *δ* < 0.005 *cm*⁻¹. This table is a small section of the list of 1629 transitions attached as Supplementary Material and the 3481 lines given in the RT supplemental list. For the room temperature list, the empirical *J*"' is rounded to the nearest integer and the experimental *E*"' is replaced with a calculated lower state energy for that value of *J*.

Fig.1

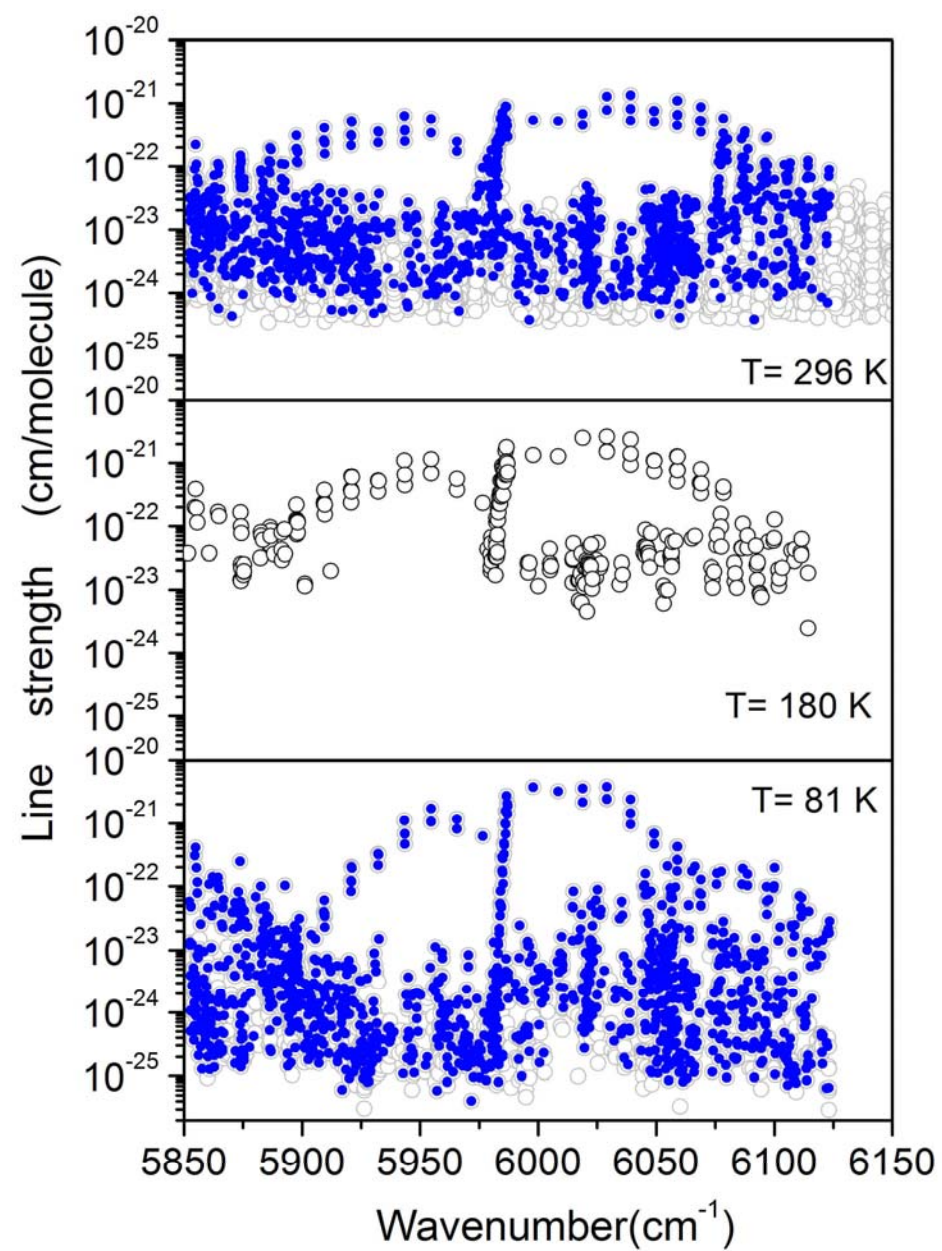


Fig.2

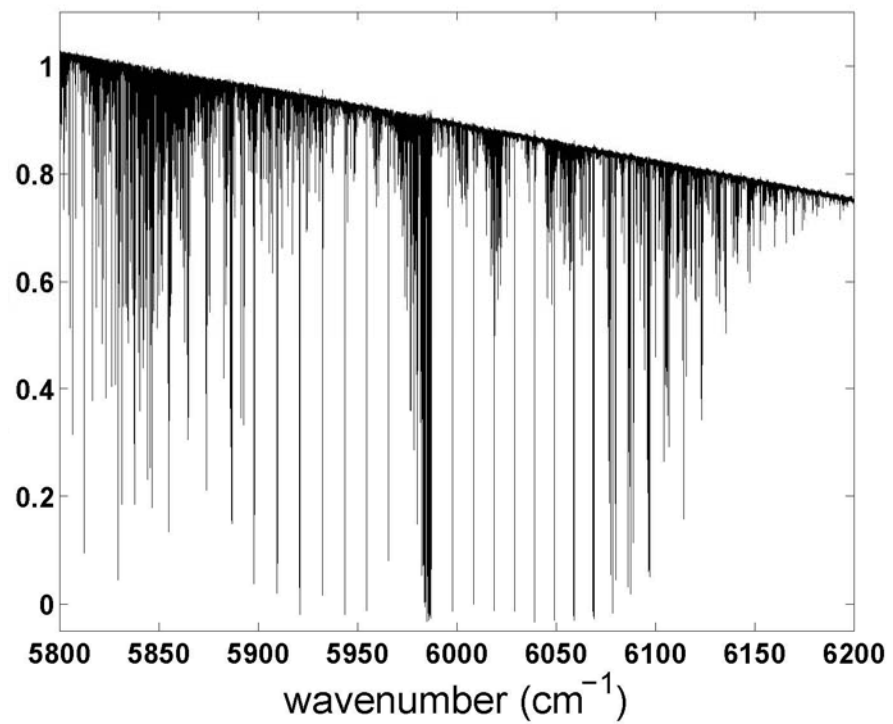
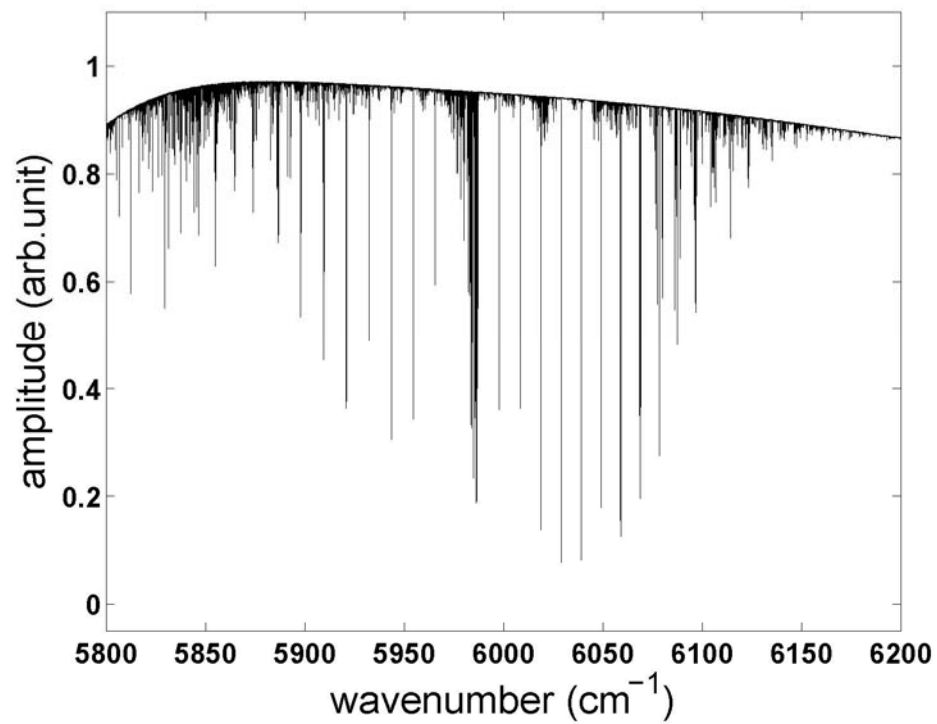


Fig.3

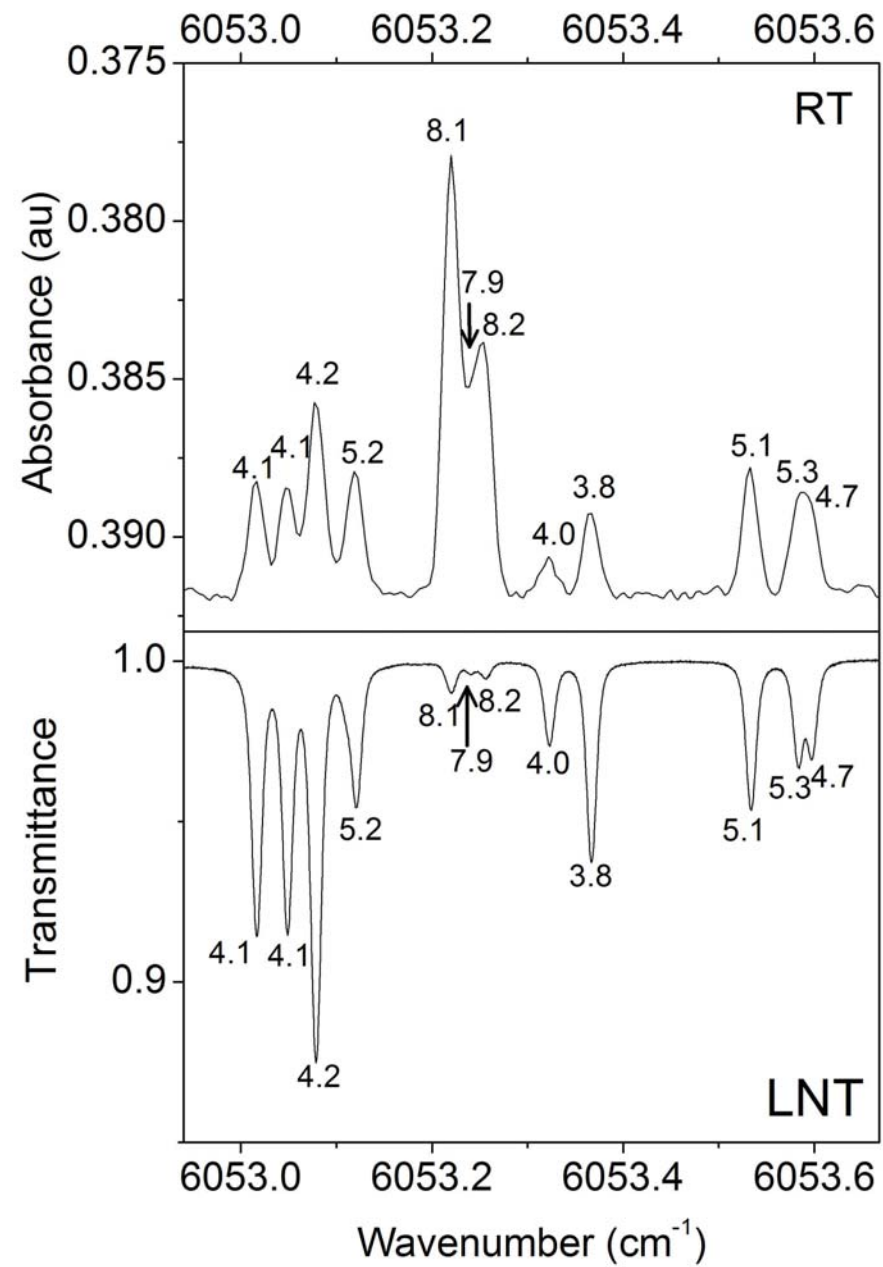


Fig.4

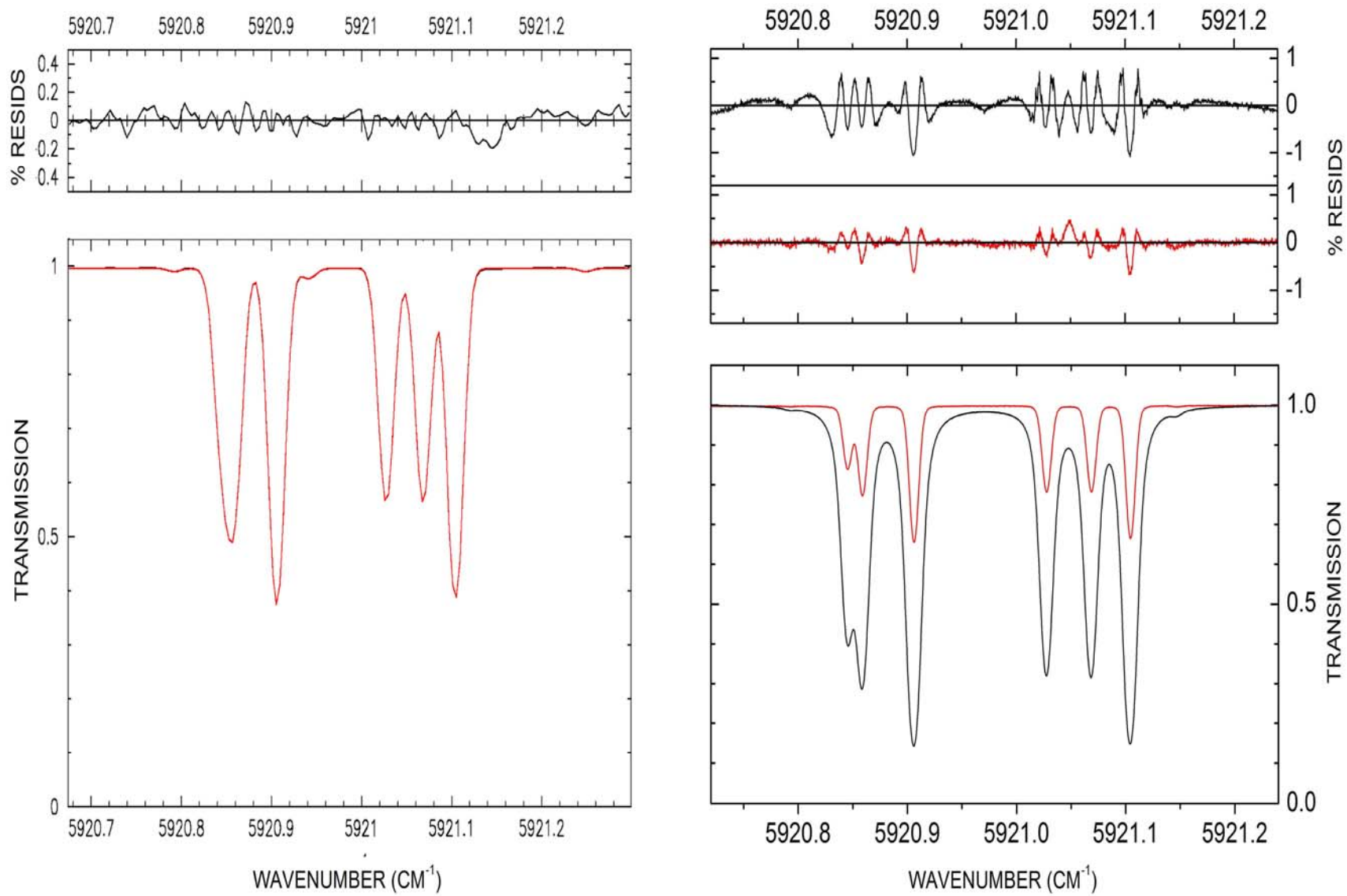


Fig.5

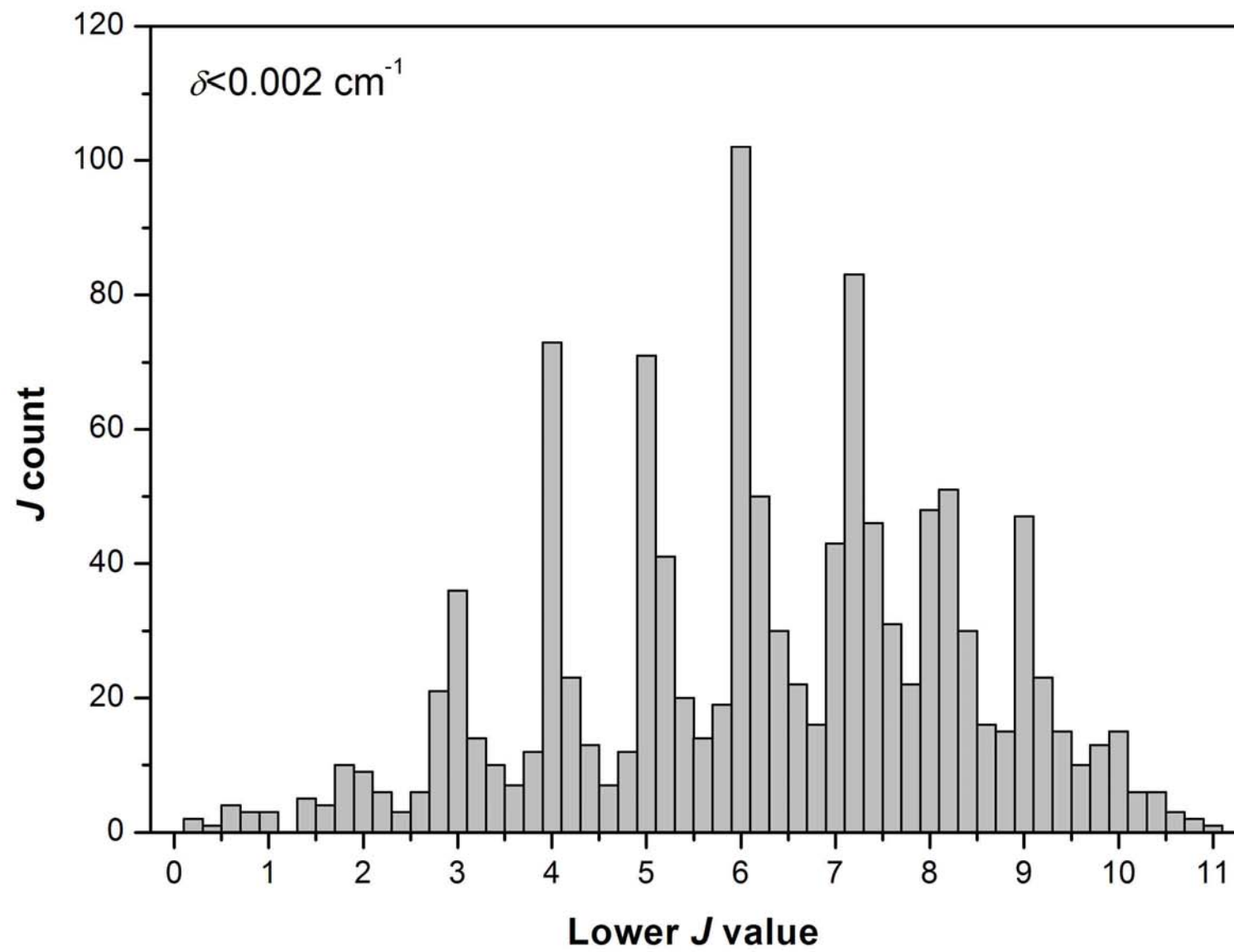


Fig.6

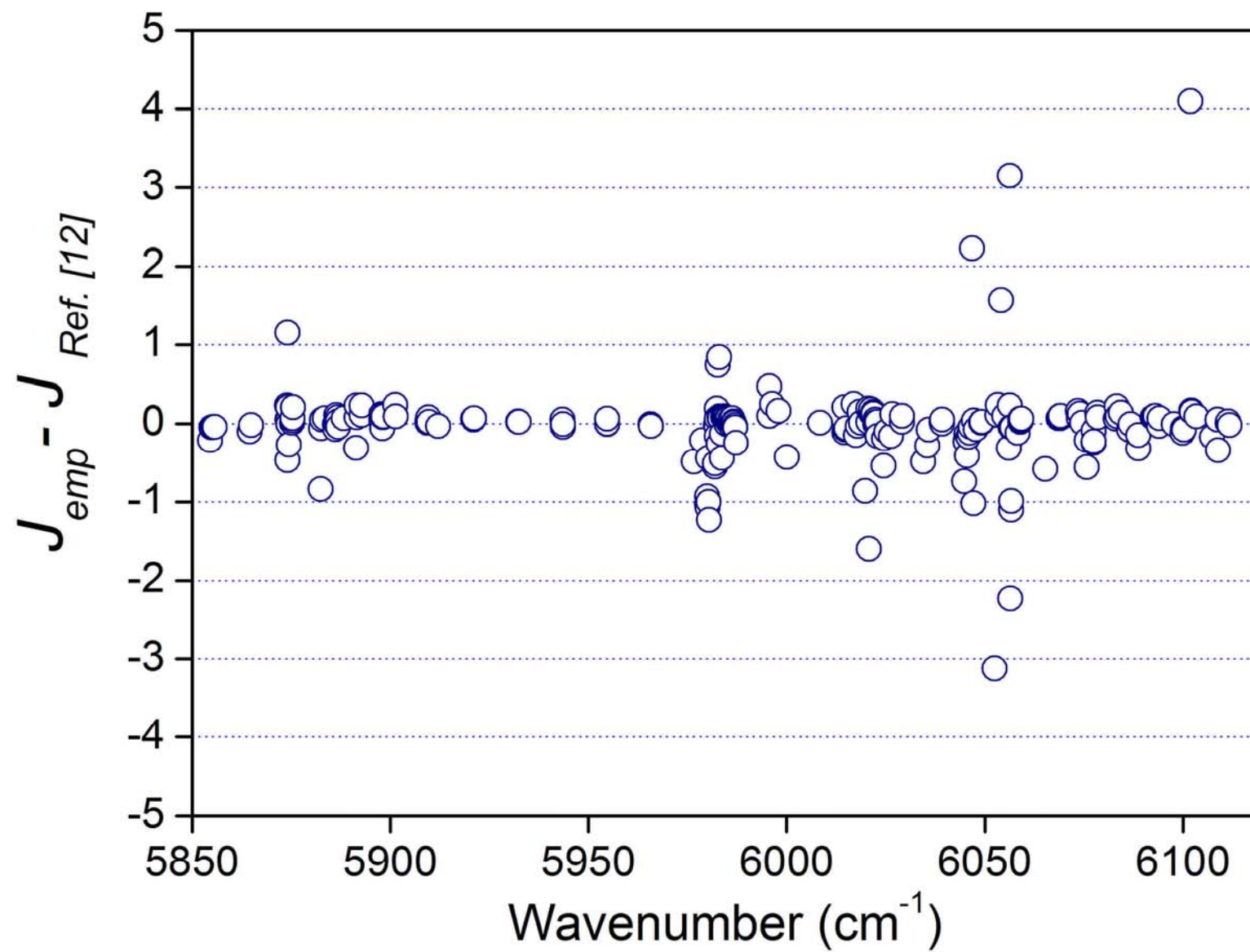


Fig.7

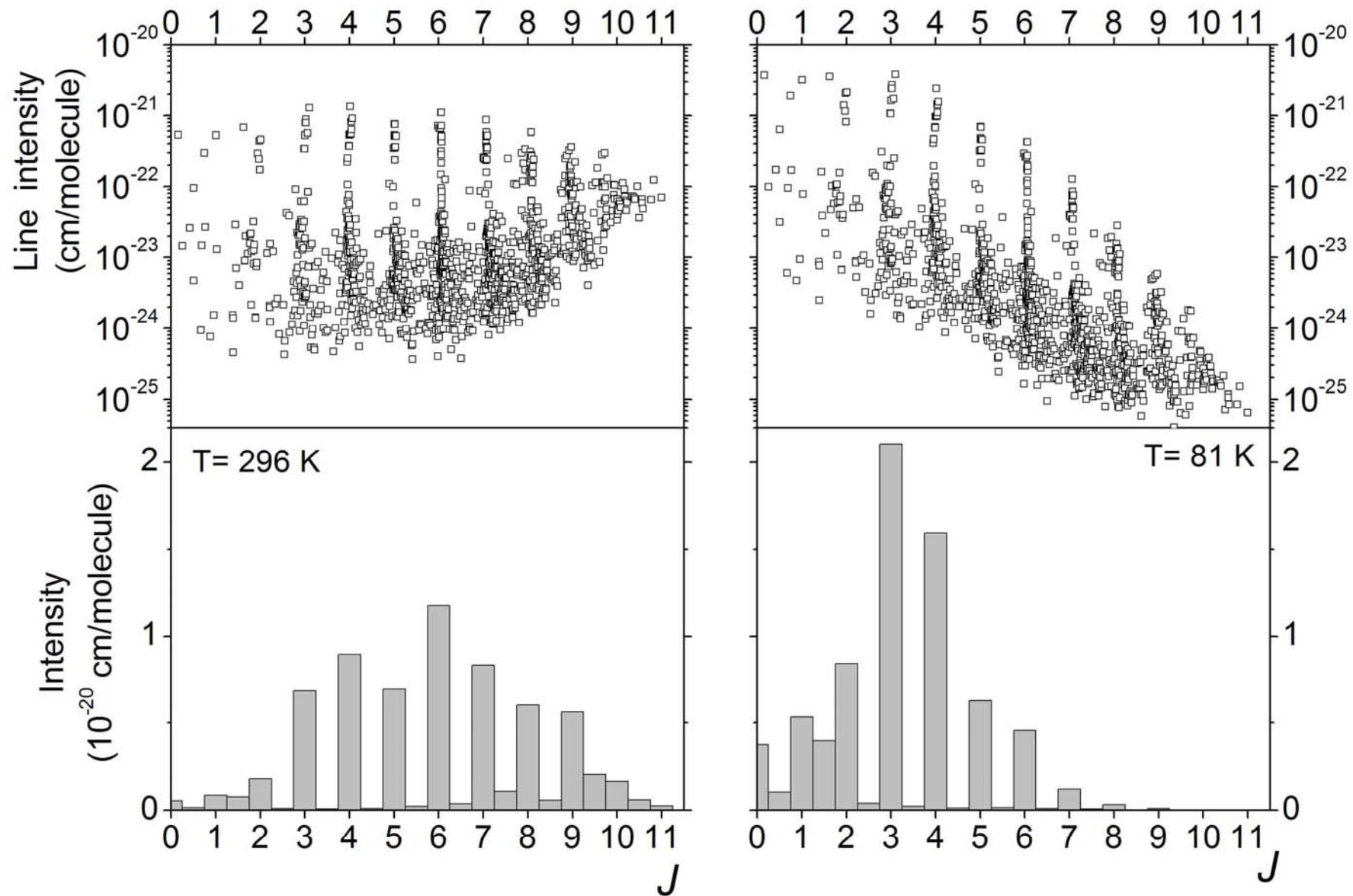
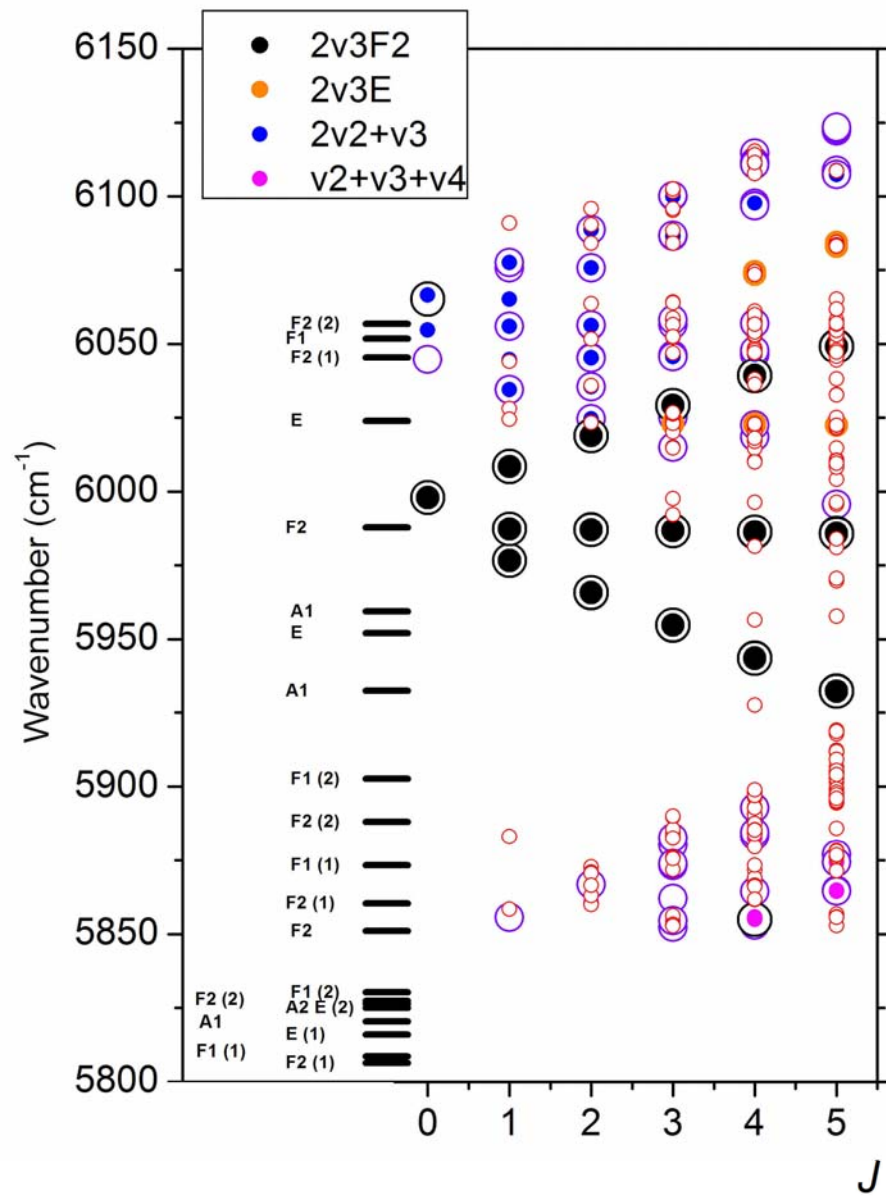
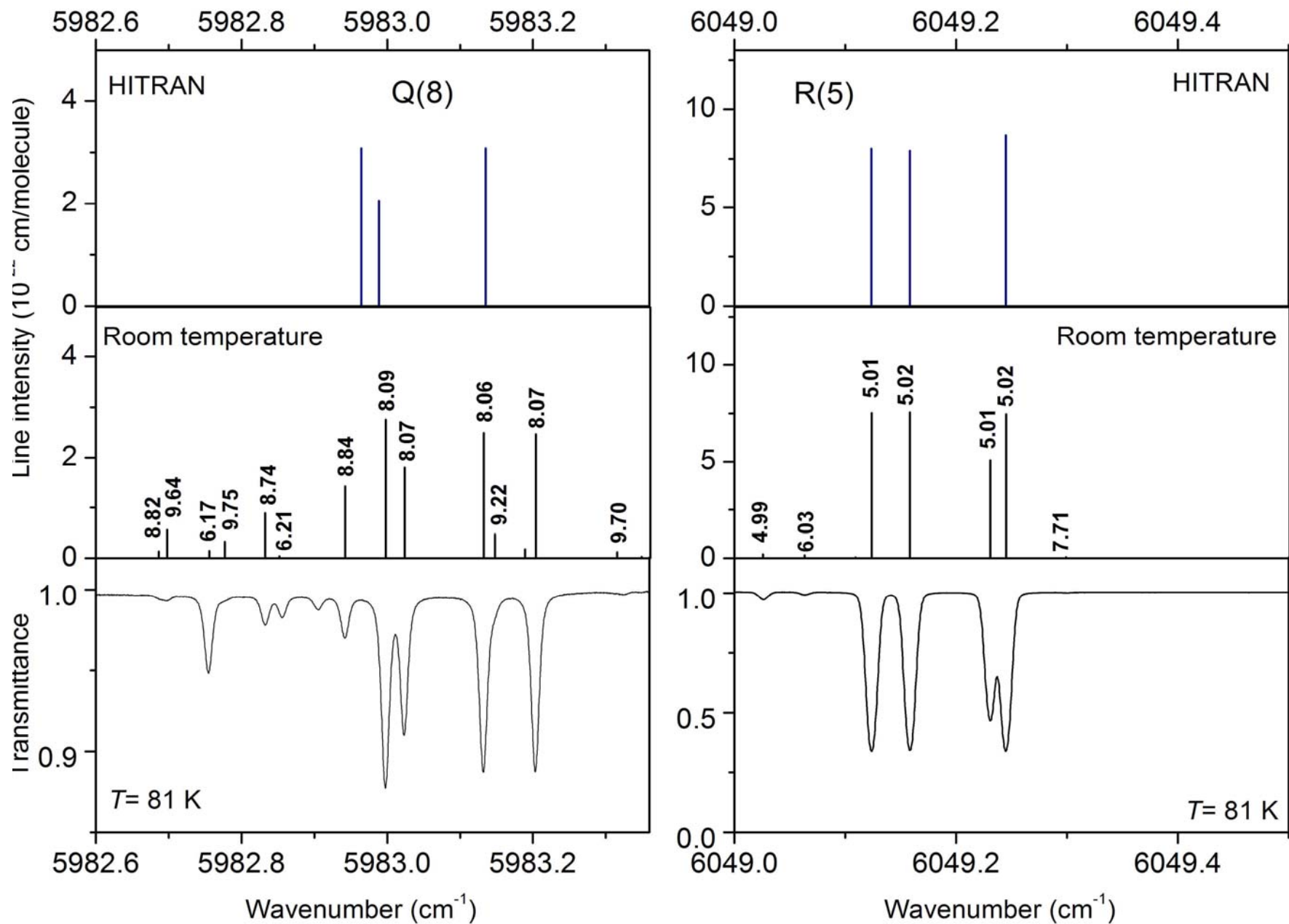


Fig.8



ig.9



Supplementary Material

[Click here to download Supplementary Material: SupMat_RT_linelist.txt](#)

Supplementary Material

[Click here to download Supplementary Material: SupMat_LNT_inelist.txt](#)